D2.2(Microwave): Report on the MW FCDR: Uncertainty

Martin Burgdorf (1), Imke Hans (1), Marc Prange (1), Jonathan Mittaz(2,3), Emma Woolliams (3)

(1) University of Hamburg, (2) University of Reading, (3) National Physical Laboratory

12th July 2019

FIDUCEO has received funding from the European Union's Horizon 2020 Programme for Research and Innovation, under Grant Agreement no. 638822

Contents

1 Introduction

1.1 Scope

This document is one of the five documents that make up the D2-2 report on "traceability chains for FCDRs". Since the original project proposal our thoughts have refined and while this document describes the "sequence of measurement standards and calibrations that is used to relate a measurement result to a reference" (the VIM definition of a traceability chain), it is not presenting this in the form of a chain.

This document provides an overview of the uncertainty analysis for the analysed sensors along with the methods to establish metrological traceability for the developed FCDRs.

This document is specifically about the Microwave FCDR (MHS, SSM-T2, AMSU-B). The document D2-2a provides an overview of the purposes of these documents and explains the basis of the effects tables.

1.2 Version Control

Version	Reason	Reviewer	Date of Issue
1.a	Final v. at end of project		July 12, 2019
1.b			
1.c			

1.3 Applicable and Reference Documents

1.3.1 D2-2 set of documents

D2-2a	Principles behind the FCDR effects table
D2-2(microwave)	Report on the MW FCDR: Uncertainty (This document)
D2-2(HIRS)	Report on the HIRS FCDR: Uncertainty
D2-2(AVHRR)	Report on the AVHRR FCDR: Uncertainty
D2-2(MVIRI)	Report on the MVIRI FCDR: Uncertainty

1.3.2 References

N. C. Atkinson: Performance of AMSU-B Flight Model 2 (FM2) during NOAA-L Post Launch Orbital Verification Tests, AMB112, Met Office, Farnborough, 24 pp., 2000

N. C. Atkinson: Calibration, Monitoring and Validation of AMSU-B, ADV SPACE RES, 28, 117-126, 2001

N. C. Atkinson and M. V. Ricketts, Calibration of E109 PRTs, July 1992 to April 1994, Met O Branch Working Paper No. 63, 24pp., April 1994

R. Bonsignori: In-Orbit Verification of MHS Spectral Channels Co-registration Using the Moon, SPIE Optics + Photonics, Conference on "Earth Observing Systems XXII", San Diego, 6-10 August 2017

M. Burgdorf, I. Hans, M. Prange, T. Lang, S. A. Buehler: Inter-channel uniformity of a microwave sounder in space, ATMOS MEAS TECH, 11, 4005-4014, 2018

Gencorp, Aerojet, In-flight calibration target for AMSU-B, Sept 1990

I. Hans, M. Burgdorf, V. O. John, J. Mittaz, S. A. Buehler: Noise performance of microwave humidity sounders over their life time, published as discussion paper in AMT, 2017, https://doi.org/10.5194/amt-2017-277

T. J. Hewison: A Thermal Model of Black Body Targets, November 1991, 12 pp.

MHS Level 1 Product Generation Specification, EUM.EPS.SYS.SPE.990006, 9/17, 2013, 89pp.

NOAA KLM Users Guide – June 2014 Revision, https://www1.ncdc.noaa.gov/pub/data/satellite/publications/podguides/N-15%20thru%20N-19/pdf/0.0%20NOAA%20KLM%20Users%20Guide.pdf

M. V. Ricketts and N. C. Atkinson: AMSU-B F3 EMC Susceptibility Tests carried out in July 1998, 23 pp.

M. V. Ricketts and N. C. Atkinson: Pre-shipment EMC Susceptibility Tests for AMSU-B FM2 (August 1999), 6 pp.

R. W. Saunders, T. J. Hewison, S. J. Stringer, N. C. Atkinson: The Radiometric Characterization of AMSU-B, IEEE TRANSACTIONS ON MICROWAVE THEORY AND TECHNIQUES, 43, 760-771, 1995

1.4 Glossary

AAPP	**A**TOVS and **A**VHRR **p**re-processing **p**ackage
AMSU-B	**A**dvanced **m**icrowave **s**ounding **u**nit-B
ATOVS	**A**dvanced **T**IROS-N **o**perational **v**ertical **s**ounder
AVHRR	**A**dvanced **v**ery **h**igh **r**esolution **r**adiometer
CDR	**C**limate **d**ata **r**ecord
DMSP	**D**efense **m**eteorological **s**atellite **p**rogram
DSV	**D**eep **s**pace **v**iew
ECV	**E**ssential **c**limate **v**ariable
EUMETSAT	**Eu**ropean organization for the exploitation of **met**eorological **sat**ellites
FCDR	**F**undamental **c**limate **d**ata **r**ecord
IFOV	**I**nstantaneous **f**ield **o**f **v**iew
IWCT	**I**nternal **w**arm **c**alibration **t**arget
LECT	**L**ocal **e**quator **c**rossing **t**ime
LSB	**L**ower **s**ide**b**and
MetOp	**Met**eorological **Op**erational Satellite
MHS	**M**icrowave **h**umidity **s**ounder
MW	**M**icro**w**ave
NEdT	**N**oise **e**quivalent **d**ifferential **t**emperature
NetCDF	**N**etwork **c**ommon **d**ata **f**ormat
NOAA CLASS	**N**ational **o**ceanic and **a**tmospheric **a**dministration's **c**omprehensive **l**arge-**a**rray **s**tewardship **s**ystem
NPP	**N**ational **p**olar-orbiting **p**artnership
NWP	**N**umerical **w**eather **p**rediction
POES	**P**olar **o**rbiting **e**nvironmental **s**atellites
PRT	**P**latinum **r**esistance **t**hermometer
RFI	**R**adio **f**requency **i**nterference
SNO	**S**imultaneous **n**adir **o**verpass
SSM/T-2	**S**pecial **s**ensor **m**icrowave water vapor profiler
USB	**U**pper **s**ide**b**and
UTH	**U**pper **t**ropospheric **h**umidity

VIM	**V**ocabulaire **i**nternational de **m**étrologie

2 General overview

2.1 FIDUCEO effects tables

In FIDUCEO we have defined an effects table, which describes

- the uncertainty associated with a given effect
- the sensitivity coefficient required to propagate uncertainties associated with that effect to uncertainties associated with the measurand (Earth radiance, reflectance or brightness temperature)
- the correlation structure over spatial, temporal and spectral scales for errors from this effect

The concepts behind the effects tables are described in D2-2a. In this document we provide a discussion of the effects tables and uncertainty propagation for a single instrument series; here the AMSU-B and MHS FCDRs.

3 The microwave instruments

The microwave FCDR is produced for the microwave humidity sounder series of sensors from SSM/T2 (1994-2008), AMSU-B (1998 – present) and MHS (2005 – present) which fly on-board the National Oceanic and Atmospheric Administration's (NOAA's) Polar Orbiting Environmental Satellites (POES). These sensors observe the water vapour absorption line at 183 GHz, though the exact channel frequency positions differ from sensor to sensor, and in particular for the different instrument generations. The satellite orbits the Earth 14 times each day from 830 km above its surface. The instruments are all cross-track scanners, observing the Earth in scan lines, with the along-track resolution provided by the satellite's movement. Except for SSM/T2, the IFOV of each channel is approximately 19.2 milliradians (1.1°) leading to a circular instantaneous field of view size close to 15.9 km at nadir for a nominal altitude of 833 km. There are 90 Earth samples per scan and per channel for a swath width of ± 1078 km (sampling time of 19.0 ms).

The microwave radiometers are heterodyne receivers, where the received radio frequency ν_s is down converted to a lower intermediate frequency ν_{IF} with a local oscillator (LO) at a specified and precisely controlled frequency ν_{LO} and then amplified and filtered. The output at a frequency ν_{IF} may be produced by a signal at either of *two* frequencies $\nu_S = \nu_{LO} \pm \nu_{IF.}$

For a given LO frequency, a mixer which produces output over the intermediate frequency range from ν(min) to ν(max) will therefore respond to input signals in the range from ν_{LO} + ν(min) to ν_{LO} + ν(max) and to signals in the range from ν_{LO} – ν(max) to ν_{LO} – ν(min). There are *two* bands of receivable signal frequencies, placed on either side of the LO frequency.

The band from ν_{LO} + ν(min) to ν_{LO} + ν(max) is conventionally referred to as the Upper Side Band (USB). The band from ν_{LO} – ν(max) to ν_{LO} – ν(min) is referred to as the Lower Side Band (LSB). A receiver system, which responds to both of them, is called a *double-sideband receiver.* AMSU-B 18-20 are examples for channels that are configured for double-sideband operation. The gain transfer functions, i.e. the equivalent of the

relative spectral response functions of instruments operating at optical wavelengths, of the LSB and the USB are mirror images, i. e. their values are the same for $\nu_{LO} + \nu$ and $\nu_{LO} - \nu$. They are known from tests on ground.

The microwave instrument calibration is based upon the measurement of cold space (at the temperature of the cosmic microwave background) and of an internal warm blackbody target (IWCT). This calibration sequence is performed once every scanline; i.e. once every 8/3 seconds (8 seconds for SSM/T-2). During one scan, the instrument observes deep space (DSV) and the IWCT at four different scan positions in each case. (SSM/T-2 dwells at scan position 130.5° for the IWCT and 229.5° for the DSV.) The IWCT of MHS is equipped with five platinum resistance thermometers (PRTs), as opposed to the seven PRTs for the AMSU-B instrument and two PRTs for SSM/T-2.

Table 1 provides an instrument package breakdown for all microwave sounders considered by FIDUCEO.

Table 1 *SSM-T2, AMSU-B, and MHS instrument package breakdown*

Instrument/Antenna package	***SSM-T2***	***AMSU-B***	***MHS***
Channel frequencies (bandwidths) (GHz)	91.655±1.25 150.0±1.25 183.31±1.00 183.31±3.00 183.31±7.00	89.0±0.9 (1) 150.0±0.9 (1) 183.31±1.00 (0.5) 183.31±3.00 (1) 183.31±7.00 (2)	89.0 (2.8) 157.0 (2.8) 183.311±1.0 (0.5) 183.311±3.0 (1) 190.311 (2.2)
Number of warm target PRTs	2	7	5
Number of warm target views per scan line	4	4	4
Number of cold space views per scan line	4	4	4
Beamwidth (degrees)	6.0 at 91.655 GHz 3.7 at 150 GHz 3.3 at all other channels	1.1	1.1
Scan range (degrees)	±40.5	±48.95	±49.44

3.1 The MW measurement function

3.1.1 The AAPP code

Operationally, and for current reanalyses, the analysis is currently performed using the AAPP (ATOVS [Advanced TIROS-N {Television and InfraRed Observation Satellite} Operational Vertical Sounder] and AVHRR [Advanced Very High Resolution Radiometer] Pre-processing Package) code. AAPP may be used to process global or regional NOAA, MetOp or NPP data, for example AMSU, HIRS and MHS level 1b data from the NOAA archives. For the MW-FCDR production, we are basing the analysis on the AAPP code, but with modification of some of the calibration parameters from our harmonisation process.

In the sections below we discuss some ways in which the AAPP code is a simplification. However at present no attempt is made to correct for these simplifications.

3.1.2 The measurement function from AAPP

The measurement function from the AAPP, written for the measurand Earth radiance, is:

$$L_{E,i} = \frac{(L_{ME,i} - g_{S,i}L_{CMB} - g_{Pl,i}L_{Pl})}{g_{E,i}} + \Delta L_{pol}$$

Eq 3-1

Where,

$L_{E,i}$ Is the Earth radiance for a pixel i

$L_{\mathrm{ME},i}$ Is calculated from the measured Earth radiance for that pixel, the radiance from space, and the satellite platform that are observed in the side-lobes of the antenna gain pattern (AGP)

L_{CMB} Is the radiance of the cosmic microwave background

L_{Pl} Is the radiance of the satellite platform. The AAPP code makes the assumption that the reflectivity of the platform is one, i.e. that $L_{\mathrm{Pl}} = L_{\mathrm{E}}$ (Section 3.1.4).

The g terms represent the fraction of the sphere subtended by the Earth, space and the satellite platform when viewing pixel i, weighted by the antenna gain pattern, i.e.

$$g_{\mathrm{E},i} = \frac{\int_{\mathrm{Earth},\,i} AGP(\Omega)\,\mathrm{d}\Omega}{\int_{4\pi} AGP(\Omega)\,\mathrm{d}\Omega} = 1 - g_{\mathrm{S},i} - g_{\mathrm{Pl},i}\,,$$

Eq 3-2

$$g_{\mathrm{S},i} = \frac{\int_{\mathrm{Space},\,i} AGP(\Omega)\,\mathrm{d}\Omega}{\int_{4\pi} AGP(\Omega)\,\mathrm{d}\Omega}\,,$$

Eq 3-3

$$g_{\mathrm{Pl},i} = \frac{\int_{\mathrm{Platform},\,i} AGP(\Omega)\,\mathrm{d}\Omega}{\int_{4\pi} AGP(\Omega)\,\mathrm{d}\Omega}\,,$$

Eq 3-4

Where,

$AGP(\Omega)$ Is the antenna gain pattern as a function of solid angle, and the upper integrals are over the solid angles subtended by the Earth, by space and by the satellite platform, respectively.

The measured Earth radiance, $L_{\mathrm{ME},i}$ in Eq 3-1, is given from the measured Earth counts and the instantaneous gain calculated from the calibration with the IWCT and space views, as well as corrections for nonlinearity and for polarisation effects:

$$L_{ME,i} = L_{MIWCT} + \frac{L_{MIWCT} - L_{MS}}{\bar{C}_{IWCT} - \bar{C}_S}\left(C_{E,i} - \bar{C}_{IWCT}\right) + \Delta L_{nl} + 0$$

Eq 3-5

Where,

L_{MIWCT}	Is the band-integrated measured radiance of the internal warm calibration target, see below
L_{MS}	Is the band-integrated measured radiance of deep space, this includes contributions from other elements in the antenna side lobes, see below
$\bar{C}_{\mathrm{IWCT}}$	Is the averaged count signal when measuring the IWCT. This has been calculated as a weighted average from calibration measurements over several scanlines
$\bar{C}_{\mathrm{S}}$	Is the averaged count signal when measuring deep space. This has been calculated as a weighted average from calibration measurements over several scanlines
$C_{\mathrm{E},i}$	Is the count signal when measuring the Earth
ΔL_{nl}	Is a nonlinearity correction, see below
ΔL_{pol}	Is a polarisation correction, see below
+0	Represents the extent to which this equation form is an approximation.

The measured IWCT radiance is calculated from a modified Planck equation, as:

$$L_{MIWCT} = L_{BB}(\nu_{ch}, A, b, T_{IWCT}, \delta T_{ch})+0$$

$$L_{BB} = \frac{2h\nu_{ch}^3}{c^2\left(e^{\frac{h\nu_{ch}}{k_B(A+b(T_{IWCT}+\delta T_{ch}))}} - 1\right)}$$

Eq 3-6

Where,

h	Is the Planck constant
c	Is the speed of light
k_B	Is the Boltzmann constant
ν_{ch}	Is the effective frequency of the channel
A, b	Are band-correction coefficients which describe the difference between a Planck function evaluated at the centre frequency (183 GHz) and the average of the Planck functions at two frequencies above and below the centre frequency. They are $A=0, b=1$ for all channels except for channels 19 and 20 of AMSU-B and channel H4 of MHS.
T_{IWCT}	Is the temperature measured by the platinum resistance thermometers (PRTs) on the IWCT (a weighted average)

δT_{ch} Is a channel-dependent warm target bias correction that accounts for the contamination by radiation originating in the shroud or local oscillator and other sources of bias. Eq 3-6 makes a number of simplifications discussed in Section 3.1.4.1. The plus zero term accounts for these simplifications.

The band-integrated measured space radiance is calculated from the cosmic microwave background radiation (determined from Planck's law for the temperature of the CMB, $T_{CMB\,0}$), and a space-view antenna pattern correction for that channel. This space-view antenna pattern correction can be calculated in a similar way to that for the Earth view (see discussion in Section 3.1.4.3) taking into account the radiation of the Earth and the satellite that enters through the side lobes by an additive correction term ΔT_c. This involves certain simplifications (Section 3.1.4.3) and the plus zero term accounts for them. See also section 3.1.5.

$$L_{MS} = L_{SV}(\nu_{ch}, A_s, b_s, T_{CMB\,0}, \Delta T_c) + 0$$

$$L_{SV} = \frac{2h\nu_{ch}^3}{c^2\left(e^{\frac{h\nu_{ch}}{k_B(A_s + b_s(T_{CMB\,0} + \Delta T_c))}} - 1\right)} \qquad \textit{Eq 3-7}$$

The space view and IWCT view counts are averaged in a weighted rolling average over seven scan lines, thus:

$$\bar{C}_{IWCT} = \frac{\sum_{k=-3}^{3}\left(1 - \frac{|k|}{n+1}\right)C_{IWCT,k}}{4}, \qquad \bar{C}_S = \frac{\sum_{k=-3}^{3}\left(1 - \frac{|k|}{n+1}\right)C_{S,k}}{4}.$$

Eq 3-8

The non-linearity correction is given by:

$$\Delta L_{nl} = \frac{q_{nl}(C_{E,i} - \bar{C}_S)(C_{E,i} - \bar{C}_{IWCT})(L_{MIWCT} - L_{MS})^2}{(\bar{C}_{IWCT} - \bar{C}_S)^2}$$

Eq 3-9

Where q_{nl} is the nonlinearity coefficient and other terms have the same meaning as given above. The nonlinearity coefficient determined through pre-flight calibration is only significant for channel 1; the term is considered suitable for harmonisation (Section 3.1.5), in particular for channel 1.

The polarisation correction is given by

$$\Delta L_{pol} = \frac{\alpha(L_{MIWCT} - \hat{L}_{E,i})(\cos(2\vartheta_{E,i}) - \cos(2\vartheta_S))}{2} + 0$$

Eq 3-10

Where, α, a property of the mirror, is one minus the ratio of reflectivity at 90° and nadir. The angles $\vartheta_{E,i}, \vartheta_S$ are the antenna angles for the ith Earth view pixel and the space view pixel, respectively and $\hat{L}_{E,i}$ is the uncorrected Earth view radiance and the + 0 represents the extent to which this equation is an approximation (section 3.1.3).

3.1.3 RF interference

For AMSU-B, and to different extent for different channels, there is radiofrequency interference in particular from the S-band transmitters on NOAA-15. For these channels we need to consider ignoring affected data, correcting affected data or increasing the uncertainty of affected data, depending on the scale of the

interference and the availability of other information. These considerations rely on the description of RF interference in EMC test reports by Ricketts and Atkinson (1998 and 1999) as well as the publication in Adv. Space Res. by Atkinson (2001). The exact numbers can be found in Appendix M of the KLM User's Guide (2014). An additional complication comes from the fact that even when the RFI causes a stable bias in counts, this bias may still vary considerably when expressed in brightness temperature. This is similar to the NEΔT variations documented in Hans et al. (2017).

Where a correction is made, it applies to the raw counts, and the calibration described above remains the same.

These points are further discussed in Section 4.6.

3.1.4 Simplifications in the AAPP approach

The AAPP approach makes a number of simplifications, which are discussed here.

3.1.4.1 Measured IWCT radiance

The measured IWCT radiance is calculated using Eq 3-6 from a modified Planck equation, where the blackbody temperature is replaced by $A+b\left(T_{\mathrm{IWCT}}+\delta T_{ch}\right)$ (Eq. (5) in Saunders et al., 1995). A and b represent the difference between the monochromatic Planck function at the centre frequency and the observation at two frequencies either side of the central frequency. This difference has been calculated analytically and is given as 0,1 for most channel except for those where the two frequencies are well separated. The uncertainty on A,b due to the approximation to 0,1 is negligible.

The term δT_{ch} is a channel-dependent warm-bias correction and is supposed to reflect the contamination by radiation originating from the S/C and the Earth limb (Sect. 5.1.2.2.2 in EUM.EPS.SYS.SPE.990006). As the viewing direction for the IWCT pixels is opposite to nadir, there is no contamination from the Earth limb, and the correction is always zero. The only exception is channel 20 of AMSU-B on NOAA-17, where it is -0.16 K. It is unclear why one channel on one instrument should be different w. r. t. warm bias correction from all others.

Eq 3-6 does not account for the radiation of the shroud. There are also further approximations in the measured IWCT radiance due to temperature drifts and gradients on the IWCT and reflections onto the IWCT from the local oscillator. These are treated as uncertainties and discussed in Section 4.3.

3.1.4.2 Platform radiance

The measurement function, Eq 3-1, includes terms for the antenna pattern side lobe observations of the platform and of space. This includes the radiance of the platform, L_{pl}. This platform radiance is poorly known (and probably the platform has a complex mix of temperatures and emissivities). The AAPP makes the simplification of assuming that the platform is highly reflective and therefore the best estimate of the platform radiance is the Earth radiance. This approximation is fundamentally wrong.

3.1.4.3 Measured space-view radiance

The band-integrated measured space-view radiance is

$$L_{MS} = \hat{g}_S L_{CMB\,0} + \hat{g}_E \hat{L}_E + \hat{g}_{Pl} \hat{L}_{Pl}$$

Eq 3-11

where the $\hat{g}$ terms are similar to the g terms in Eq 3-2 to Eq 3-4, but for the space view and the radiances are the band-integrated radiances of the cosmic microwave background, the Earth, and the platform respectively. Note that the Earth and platform radiances are not necessarily the same as for the Earth view as different parts of the Earth are in the sidelobes of the space view than the Earth measured for the Earth view and the platform will reflect different radiation and could be at a different temperature. Therefore they are marked with a grave accent.

Because these terms are not well known and the approximations within AAPP to this are not considered sufficient for the FCDR, we include them in ΔT_C and allow for its numerical value to be optimised as a harmonisation coefficient. This means replacing Eq 3-11 with Eq 3-7.

See appendix A.4 for a further discussion of this term.

3.1.4.4 Polarisation correction

The Eq 3-10 should be an iterative equation as it depends on the measured Earth radiance $L_{\mathrm{E},i}$. In practice AAPP simply uses the original uncorrected measured Earth radiance, $\hat{L}_{\mathrm{E},i}$ and does not recalculate this after the correction. Given the fact, however, that the largest absolute value of α is 0.0022, we do not expect a significant improvement of the measurement accuracy by carrying out the full iterative process. The maximum value of the polarisation correction amounts to a few hundred mK. AAPP does not apply a polarisation correction to data from AMSU-B.

3.1.5 Harmonisation

The process of harmonisation could be used to determine improved evaluations of the following quantities, assuming that match ups provide a more reliable estimate of these quantities than the pre-flight calibration or the tabulated values used in AAPP look up tables:

Harmonisation Coefficient	Quantity	Effect on Calibration
a_1	q_{nl}	Nonlinearity coefficient term in Eq 3-9
a_2	α	One minus mirror reflectivity ratio at 90° and at nadir in Eq 3-10
a_3	ΔT_C	Cold space bias correction in Eq 3-7

The process of harmonisation would use match-ups between sensors, taking one sensor in the series as a reference, to provide an improved estimate of these quantities.

3.2 Measurement Function Tree Diagram

The measurement function tree diagram for the microwave sensors is given in Figure 1. The tree is designed to show the sources of uncertainty from their origin through to the uncertainty in the measurand. On the outside of the tree are the origins of the uncertainty which range from those with a physical origin such detector/electronic noise sources (which will be purely random effects) to error sources in the estimations of antenna pattern corrections. Note that we try to include all possible sources of uncertainty however small that is one of the requirements of metrological traceability.

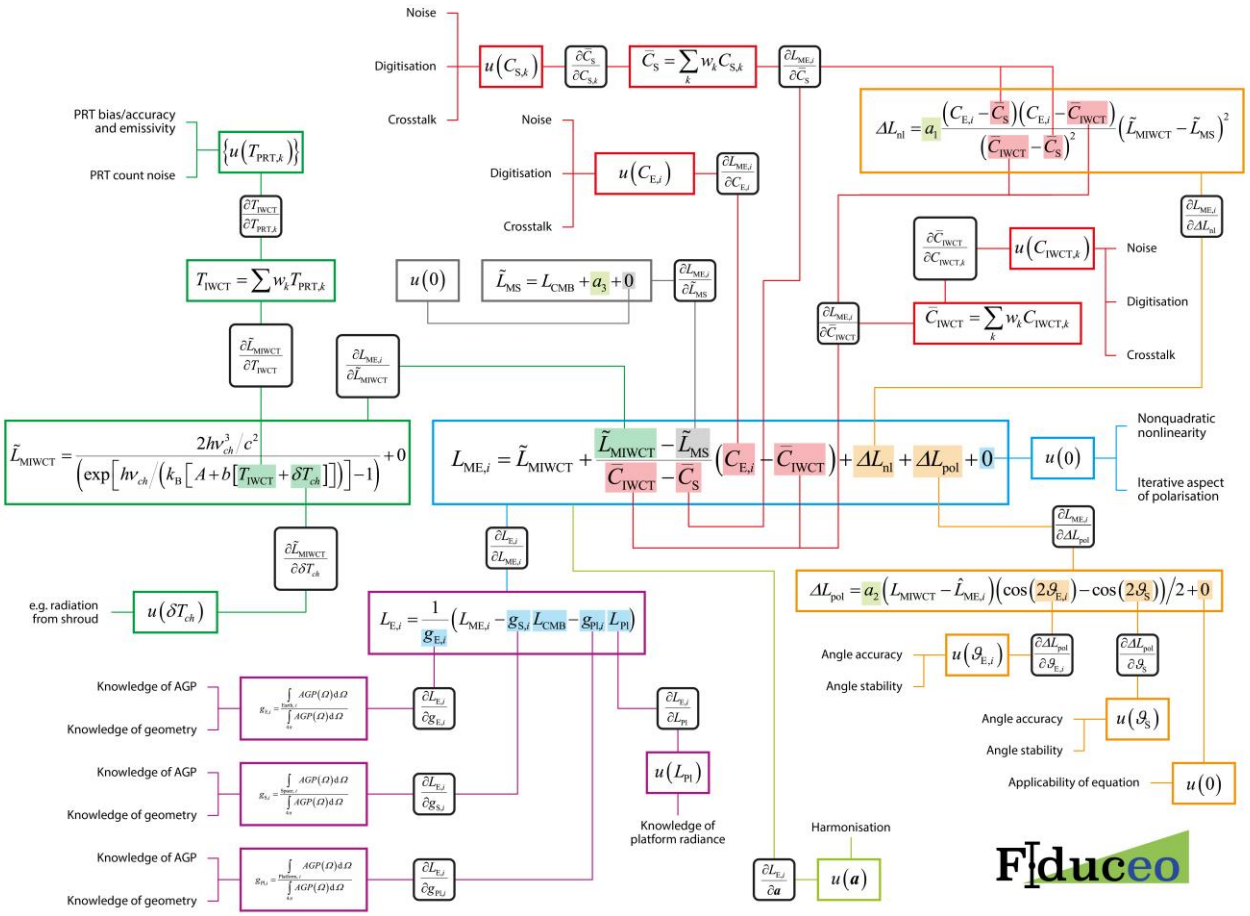

Figure 1 The measurement function tree for the microwave FCDR.

4 A discussion of different terms

In this section we consider the different sources of uncertainty and discuss the error correlation structure for this effect in the different dimensions using the Effects Tables that have been described in D2-2a. A full description of how this effect was evaluated is beyond the scope of this paper, but references are given, or details are provided in the appendices.

4.1 Noise in Earth Counts, Averaged Space Counts and Averaged IWCT Counts

The measured signal is noisy. This noise comes from a combination of noise sources in the receiver and other components of the radiometer. In addition there is a digitisation of the signal. The noise on the space and IWCT counts is hard to estimate because only a small number of observations of each are made during a typical calibration run and, due to the variation of instrument temperature around an orbit, the total flux between measurements is not constant. The Earth Count noise is even harder to estimate because it is difficult to find Earth scenes that are sufficiently uniform to estimate any Earth Count noise. This noise is therefore estimated from scaling the noise of DSV and IWCT according to the recorded Earth Counts (Hans et al., 2017). A further discussion is given in Appendix A.1.

The Earth count is observed per pixel and therefore any noise associated with it will be independent from one pixel to another (it is a purely random effect).

The Space and IWCT counts are, however, determined four times per scanline and averaged as a weighted rolling average across an averaging window of 7 scanlines (3 before and 3 after). This means that all pixels on a scanline have a fully correlated error associated with IWCT and Space observation noise and that the correlation from one scanline to another falls off as bell-shaped (see D2-2a). There is no correlation from spectral channel to spectral channel. The uncertainty associated with the averaged space and IWCT noise counts are provided every 300 scanlines as discussed in (Hans et al., 2017).

The effects tables for Microwave counts are given in Table 2.

Table 2 Effects tables for the Earth, averaged-Space and averaged-IWCT counts

Table descriptor				
Name of effect		Earth Count Noise	Averaged Space Count Noise	Averaged IWCT Count Noise
Affected term in measurement function		C_E	$\bar{C}_S$	$\bar{C}_{IWCT}$
Instruments in the series affected		All	All	All
Correlation type and form	Pixel-to-pixel [pixels]	Random	Rectangular Absolute	Rectangular Absolute
	From scanline to scanline [scanlines]	Random	Bell shaped	Bell shaped
	between images [images]	N/A	N/A	N/A
	Between orbits [orbit]	Random	Random	Random
	Over time [time]	Random	Random	Random
Correlation scale	Pixel-to-pixel [pixels]	[0]	$[-\infty, +\infty]$	$[-\infty, +\infty]$
	from scanline to scanline [scanlines]	[0]	n = 7	n = 7
	between images [images]	N/A	N/A	N/A
	Between orbits [orbit]	[0]	[0]	[0]
	Over time [time]	[0]	[0]	[0]
Channels/bands	List of channels / bands affected	All	All	All
	Correlation coefficient matrix	Identity matrix (1s down diagonal only)	Identity matrix (1s down diagonal only)	Identity matrix (1s down diagonal only)
Uncertainty	PDF shape	Digitised Gaussian	Digitised Gaussian	Digitised Gaussian
	units	Counts	Counts	Counts
	magnitude	Provided per pixel	Provided every 300 scanlines	Provided every 300 scanlines
Sensitivity coefficient		$\frac{\partial L_E}{\partial C_E}$, Eq 4-1	$\frac{\partial L_E}{\partial \bar{C}_S}$, Eq 4-2	$\frac{\partial L_E}{\partial \bar{C}_{IWCT}}$, Eq 4-3

The sensitivity coefficients are

$$\frac{\partial L_{E,i}}{\partial C_{E,i}} = \frac{\partial L_{E,i}}{\partial L_{ME,i}} \frac{\partial L_{ME,i}}{\partial \bar{C}_{E,i}} = \frac{1}{g_E}\left(\frac{L_{MIWCT} - L_{MS}}{\bar{C}_{IWCT} - \bar{C}_S} + q_{nl}\frac{(L_{MIWCT} - L_{MS})^2}{(\bar{C}_{IWCT} - \bar{C}_S)^2}\right)(2C_{E,i} - \bar{C}_{IWCT} - \bar{C}_S)$$

$$\frac{\partial L_{E,i}}{\partial \bar{C}_S} = \frac{\partial L_{E,i}}{\partial L_{ME,i}} \frac{\partial L_{ME,i}}{\partial \bar{C}_S} = \frac{(C_{E,i} - \bar{C}_{IWCT})(L_{MIWCT} - L_{MS})}{g_E(\bar{C}_{IWCT} - \bar{C}_S)^2}\left(1 + q_{nl}\frac{2C_{E,i} - \bar{C}_{IWCT} - \bar{C}_S}{\bar{C}_{IWCT} - \bar{C}_S}\right) \quad \textit{Eq 4-1}$$

$$\frac{\partial L_{E,i}}{\partial \bar{C}_{IWCT}} = \frac{\partial L_{E,i}}{\partial L_{ME,i}} \frac{\partial L_{ME,i}}{\partial \bar{C}_{IWCT}} = \frac{(C_{E,i} - \bar{C}_S)(L_{MIWCT} - L_{MS})}{g_E(\bar{C}_{IWCT} - \bar{C}_S)^2}\left(1 + q_{nl}\frac{(L_{MIWCT} - L_{MS})(2C_{E,i} - \bar{C}_{IWCT} - \bar{C}_S}{\bar{C}_{IWCT} - \bar{C}_S}\right) \quad \textit{Eq 4-2}$$

Eq 4-3

4.2 Gain transfer function (spectral response function)

The gain transfer function, equivalent to the spectral response function for visible and infrared radiometers, is in the ideal case a rectangle whose width is the bandwidth specified for each channel. The true shape is known from ground tests and cannot be checked in flight. The tests on ground with MHS for NOAA-18 and -19 had a random uncertainty of about 5 % at each frequency value. The centre frequency stability of the oscillator of MHS on NOAA-18 and -19 lies between ±35 MHz and ±92 MHz, depending on channel number. For AMSU-B the analogous numbers are ±50 MHz and ±100 MHz; this is small compared to a typical FWHM of the water line of 6 GHz.

To the flux calibration the gain transfer function and the exact value of the centre frequency are irrelevant, because they are the same for observations of the Earth and the flux standards. They matter, however, to the generation of CDRs, in particular the characterisation of the water line at 183~GHz. The value of the integral over the product of the line shape and a rectangle differs by about 0.1 K from the value of the integral over the product of the line shape and the (normalized) measured gain transfer function. The impact of an error in the centre frequency depends on the exact line shape, but because the water line is rather symmetric, the loss of signal in one side band is compensated in good approximation by a gain of signal in the other, when the centre frequency changes.

The drift of the centre frequency is caused by changes of temperature of the local oscillator. Hence it is correlated with position in orbit and local equator crossing time. The changes in centre frequency as a function of instrument temperature have been characterised during ground tests, therefore it is in principle possible to calculate corrections to the centre frequencies in flight.

Table 3 Effects tables for the gain transfer function

Table descriptor		
Name of effect		Gain transfer function
Affected term in measurement function		Not applicable
Instruments in the series affected		All
Correlation type and form	Pixel-to-pixel [pixels]	
	from scanline to scanline [scanlines]	
	between images [images]	
	Between orbits [orbit]	
	Over time [time]	Systematic with all
Correlation scale	Pixel-to-pixel [pixels]	
	from scanline to scanline [scanlines]	
	between images [images]	
	Between orbits [orbit]	
	Over time [time]	Correlated on time scale of years
Channels/ bands	List of channels / bands affected	All
	Correlation coefficient matrix	Not applicable
Uncertainty	PDF shape	Unknown
	units	
	magnitude	
Sensitivity coefficient		0

4.3 IWCT Radiance effects

Eq. 3-6 is an approximation for the IWCT measured radiance, which could more accurately be considered

$$L_{MIWCT} = \eta_{sp}\left(L_{IWCT} + \Delta L_{drift} + \Delta L_{grad} + \Delta L_{meas} + \Delta L_{vert} + (1-\varepsilon_{IWCT})L_{LO}\right) + (1-\eta_{sp})L_{shroud}$$

$$L_{IWCT} = \frac{2h\varepsilon_{IWCT}}{c^2}\int \frac{\nu^3 \xi_{ch}(\nu)}{e^{\frac{h\nu}{k_B T_{IWCT}}} - 1} d\nu \qquad \textit{Eq 4-4}$$

Eq 4-5

where,

ε_{IWCT} Is the coupling efficiency between the IWCT and the receiver

η_{sp} Is the coupling efficiency between the IWCT and the receiver

L_{IWCT} Is the band-integrated radiance of the IWCT (considered a greybody at temperature T_{IWCT} and with an emissivity $\varepsilon_{\mathrm{IWCT}}$)

$\xi_{ch}(\nu)$ Is the normalized gain transfer function (equivalent to SRF) of the channel and T_{IWCT} is the temperature of the IWCT as seen by the receiver.

$\Delta L_{\mathrm{drift}}$ Is the radiance error due to changes in the IWCT or the PRTs over time. There is also an error due to the difference between the time the PRTs are read and the time the instrument points at the IWCT. This cannot be more than 8/3 sec, the duration of one scan; with a maximum temperature drift during an orbit of 0.1 mK/sec, this kind of drift is negligible.

ΔL_{grad} Is the radiance error due to temperature gradients in the IWCT across the IWCT

ΔL_{meas} Is the radiance error due to temperature measurement uncertainties

ΔL_{vert} Is the radiance error due to vertical gradients in the IWCT (i.e. from top to bottom of the pyramidal structure)

$(1-\varepsilon_{\mathrm{IWCT}})L_{\mathrm{LO}}$ Is the reflected (one minus emissivity) radiation from the local oscillator onto the IWCT

$(1-\eta_{\mathrm{sp}})L_{\mathrm{shroud}}$ Is the shroud radiance that reaches the receiver (feedhorn spillover)

The IWCT radiance is calculated from Eq 3-6 assuming that the IWCT is a blackbody with a temperature given by $A+b\left[T_{\mathrm{IWCT}}+\delta T_{ch}\right]$, where the A and b relate to the monochromatic approximation, rather than considering the full gain transfer function and δT_{ch} accounts for all the ΔL terms in Eq 4-4.

These terms are all considered in detail in Appendix A.2. They have different correlation structures. In summary:

η_{sp} Unknown and assumed to be one

L_{IWCT} The radiance of the IWCT is calculated from the average PRT temperature. This is both averaged over PRTs and averaged in a weighted rolling average between scanlines, see Appendix A.2.1. The noise in the PRT temperature measurement is approximately 1-15 mK (depending on instrument), with a correlation structure that relates to the 7-scanline weighted rolling average.
The radiance of the IWCT also depends on the IWCT emissivity, but this is assumed to have negligible uncertainty as it is very close to 1.

$\Delta L_{\mathrm{drift}}$ Changes in the IWCT or the PRTs over time are very difficult to measure, but they happen probably slowly. The effect is therefore fully correlated between pixels and scanlines in the same orbit file and from orbit to orbit over short timescales. There is a slow drop off in correlation over the longer timescales of the mission.

ΔL_{grad} The temperature gradients across the IWCT can be larger than 0.2 K from one side to the other (Appendix A.2.4). These gradients do not change much within an orbit or from orbit-to-orbit and the correlation structure is close to systematic. As they are correlated with the drift of the local equator crossing time, the gradients change on timescales of the order one year.

ΔL_{meas} The uncertainty associated with the absolute calibration accuracy of the PRTs is taken to be 0.1 K (rather an upper limit than a one-sigma value, Atkinson & Ricketts, 1994)

	and is a constant for the whole lifetime of the instrument (variations from this are considered in the drift term). See appendix A.2.3
ΔL_{vert}	The radiance error due to vertical gradients in the IWCT pyramidal structure was calculated with a thermal model and found to be 30 mK. (Appendix A.2.4)
$\left(1-\varepsilon_{\mathrm{IWCT}}\right)L_{\mathrm{LO}}$	As the emissivity is extremely high, this is considered negligible (Appendix A.2.2)
$\left(1-\eta_{\mathrm{sp}}\right)L_{\mathrm{shroud}}$	Is the shroud radiance that reaches the receiver (feedhorn spillover). Assumed to be negligible, because η_{SP} is close to one, and surroundings of blackbody are close to thermodynamic equilibrium. In thermodynamic equilibrium it does not matter whether the radiation arriving at the receiver comes from the blackbody or the shroud.

The non-negligible effects are listed in Table 4. All effects are fully correlated between channels because the same blackbody is observed for all channels.

Table 4 Effects tables for the IWCT band-integrated radiance

Table descriptor					
Name of effect		PRT count noise	PRT bias / accuracy (ΔL_{meas})	Thermal gradients vertical and horizontal (ΔL_{grad})	PRT long-term drift (ΔL_{drift})
Affected term in measurement function		L_{IWCT}	L_{IWCT}	L_{IWCT}	L_{IWCT}
Instruments in the series affected		All	All	All	All
Correlation type and form	Pixel-to-pixel [pixels]	Rectangular Absolute	Rectangular Absolute	Rectangular Absolute	Rectangular Absolute
	from scanline to scanline [scanlines]	Bell-shaped	Rectangular Absolute	Rectangular Absolute	Rectangular Absolute
	between images [images]	N/A	N/A	N/A	N/A
	Between orbits [orbit]	Random	Rectangular Absolute	N/A	N/A
	Over time [time]	Random	Rectangular Absolute	Bell shaped	Bell-shaped
Correlation scale	Pixel-to-pixel [pixels]	$[-\infty, +\infty]$	$[-\infty, +\infty]$	$[-\infty, +\infty]$	$[-\infty, +\infty]$
	from scanline to scanline [scanlines]	n = 7	$[-\infty, +\infty]$	$[-\infty, +\infty]$	$[-\infty, +\infty]$
	between images [images]	N/A	N/A	N/A	N/A
	Between orbits [orbit]	[0]	$[-\infty, +\infty]$	N/A	N/A
	Over time [time]	[0]	$[-\infty, +\infty]$	[n, sigma] = [2 years, 1 year]	[n, sigma] = [5 years, 2 years]
Channels/ bands	List of channels / bands affected	All	All	All	All
	Correlation coefficient matrix	Matrix of 1s everywhere	Matrix of 1s everywhere	Matrix of 1s everywhere	Matrix of 1s everywhere
Uncertainty	PDF shape	Gaussian	Gaussian	Rectangular	Rectangular
	units	kelvin	kelvin	kelvin	kelvin
	magnitude	Provided every 300 scan lines 2.4 mK (AMSU-B) 27–84 mK (MHS)	Approx. 0.1 K	Every 300 scan lines < 200 mK/° vertical, 17 mK between surface and base plate	Provided every 300 scan lines < 12 mK/year
Sensitivity coefficient		$\frac{\partial L_{\text{E}}}{\partial T_{\text{IWCT}}}$	$\frac{\partial L_{\text{E}}}{\partial T_{\text{IWCT}}}$	$\frac{\partial L_{\text{E}}}{\partial T_{\text{IWCT}}}$	$\frac{\partial L_{\text{E}}}{\partial T_{\text{IWCT}}}$

We can write, with a chain rule:

$$\frac{\partial L_E}{\partial T_{IWCT}} = \frac{\partial L_E}{\partial L_{ME}} \frac{\partial L_{ME}}{\partial L_{MIWCT}} \frac{\partial L_{MIWCT}}{\partial T_{IWCT}} \quad \text{Eq 4-6}$$

where,

$$\frac{\partial L_E}{\partial L_{MIWCT}} = \frac{\partial L_E}{\partial L_{ME}} \frac{\partial L_{ME}}{\partial L_{MIWCT}} = \frac{\eta_{sp}}{g_E}\left(1 + \frac{C_{E,i} - \bar{C}_{IWCT}}{\bar{C}_{IWCT} - \bar{C}_S} + 2q_{nl}\frac{(C_{E,i} - \bar{C}_S)(C_{E,i} - \bar{C}_{IWCT})(L_{MIWCT} - L_{MS})}{(\bar{C}_{IWCT} - \bar{C}_S)^2}\right)$$

$$\frac{\partial L_{MIWCT}}{\partial T_{IWCT}} = \frac{2h\nu_{ch}bL_{MIWCT}e^{\frac{h\nu_{ch}}{k_B(A+b(T_{IWCT}+\delta T_{ch}))}}}{k_B(e^{\frac{h\nu_{ch}}{k_B(A+b(T_{IWCT}+\delta T_{ch}))}} - 1)(A + b(T_{IWCT} + \delta T_{ch}))^2} \quad \text{Eq 4-7}$$

Eq 4-8

4.4 Space-view Radiance

The radiance for the space view is given by Eq 3-7. This includes the temperature of the cosmic microwave background and the cold space correction factor, which can be re-evaluated through harmonisation. As the uncertainty in the cosmic microwave background temperature is extremely small, and as the harmonisation process is considered separately (Section 5), no effects table is provided for space-view radiance.

4.5 Polarisation correction

The polarisation correction is given by Eq 3-10. One minus the mirror reflectivity ratio at 90° and nadir, α, can be re-determined through harmonisation and is therefore discussed separately. The other quantities are the angles $\vartheta_{E,i}, \vartheta_S$ and the difference between the measured IWCT radiance and the uncorrected Earth view radiance, and the + 0 term.

In principle, because of the potentially iterative nature of this correction (Section 3.1.4.4) there is a correlation between this term and all the other terms. However, in practice this is not calculated iteratively and we will ignore the correlation. The plus zero term in this equation includes the approximation made by ignoring this iteration.

We therefore consider only the uncertainties associated with the two viewing angles and with the form of the equation, the + 0. There will be both systematic and random effects in the determination of the angles. We have estimated the random error to be 0.04° and the systematic error to be 0.07° from other studies (check of pointing requirements on ground and analysis of Moon intrusions in the deep space view during flight), see appendix. The term is calculated separately for each pixel, but is correlated between channels.

We assume that there are separate errors in the Earth and Space views and that these are not correlated with each other. The space view occurs once per scanline and is averaged over 7 scanlines. The same error is present at all channels.

Table 5 Effects tables for the polarisation correction

Table descriptor						
Name of effect		Angle systematic in ϑ_E	Angle random in ϑ_E	Angle systematic in ϑ_S	Angle random in ϑ_S	+ 0 term
Affected term in measurement function		ΔL_{pol}	ΔL_{pol}	ΔL_{pol}	ΔL_{pol}	ΔL_{pol}
Instruments in the series affected		All	All	All	All	All
Correlation type and form	Pixel-to-pixel [pixels]	Rectangular Absolute	Bell shaped	Rectangular absolute	Rectangular absolute	Rectangular Absolute
	from scanline to scanline [scanlines]	Rectangular Absolute	Random	Rectangular absolute	Bell shaped	Rectangular Absolute
	between images [images]	N/A	N/A	N/A	N/A	N/A
	Between orbits [orbit]	Rectangular Absolute	Random	Rectangular Absolute	Random	Rectangular Absolute
	Over time [time]	Rectangular Absolute	Random	Rectangular Absolute	Random	Rectangular Absolute
Correlation scale	Pixel-to-pixel [pixels]	$[-\infty, +\infty]$	[5]	$[-\infty, +\infty]$	$[-\infty, +\infty]$	$[-\infty, +\infty]$
	from scanline to scanline [scanlines]	$[-\infty, +\infty]$	[0]	$[-\infty, +\infty]$	[7]	$[-\infty, +\infty]$
	between images [images]	N/A	N/A	N/A	N/A	N/A
	Between orbits [orbit]	$[-\infty, +\infty]$	[0]	$[-\infty, +\infty]$	[0]	$[-\infty, +\infty]$
	Over time [time]	$[-\infty, +\infty]$	[0]	$[-\infty, +\infty]$	[0]	$[-\infty, +\infty]$
Channels / bands	List of channels / bands affected	All	All	All	All	All
	Correlatn. coefficient matrix	Matrix of 1s everywhere	Matrix of 1s everywhere	Matrix of 1s everywhere	Matrix of 1s everywhere	Matrix of 1s everywhere
Uncertainty	PDF shape	Gaussian	Gaussian	Gaussian	Gaussian	Rectangular
	units	radians	radians	radians	radians	radiance
	magnitude	0.07° = 0.00122 rad	0.04° = 0.00070 rad	0.07° = 0.00122 rad	0.02° = 0.00040 rad	

Sensitivity coefficient	$\frac{\partial L_E}{\partial \vartheta_E}$,	$\frac{\partial L_E}{\partial \vartheta_E}$	$\frac{\partial L_E}{\partial \vartheta_S}$	$\frac{\partial L_E}{\partial \vartheta_S}$	

The sensitivity coefficients are

$$\frac{\partial L_E}{\partial \vartheta_E} = \frac{\partial L_E}{\partial L_{ME}} \frac{\partial L_{ME}}{\partial \Delta L_{pol}} \frac{\partial \Delta L_{pol}}{\partial \vartheta_E} \quad \text{Eq 4-9}$$

$$\frac{\partial L_E}{\partial \vartheta_S} = \frac{\partial L_E}{\partial L_{ME}} \frac{\partial L_{ME}}{\partial \Delta L_{pol}} \frac{\partial \Delta L_{pol}}{\partial \vartheta_S} \quad \text{Eq 4-10}$$

where,

$$\frac{\partial L_E}{\partial L_{ME}} \frac{\partial L_{ME}}{\partial \Delta L_{pol}} = \frac{1}{g_E} \quad \text{Eq 4-11}$$

$$\frac{\partial \Delta L_{pol}}{\partial \vartheta_{E,i}} = -\alpha (L_{MIWCT} - \hat{L}_{ME,i}) \sin(2\vartheta_{E,i}) \quad \text{Eq 4-12}$$

$$\frac{\partial \Delta L_{pol}}{\partial \vartheta_{S,i}} = \alpha (L_{MIWCT} - \hat{L}_{ME,i}) \sin(2\vartheta_{S,i}) \quad \text{Eq 4-13}$$

4.6 RF Interference

4.6.1 RF Interference on NOAA-15

AMSU-B on NOAA-15 has experienced major problems due to RF interference. A correction scheme has been made available that can correct RFI biases to an absolute accuracy of approximately ±0.3 K for channel 16, ±1 K for channels 17 and 18 and ±2 K for channels 19 and 20. These corrections are of course only necessary, when the satellite data transmitters are active. (Atkinson, 2001)

4.6.2 RF Interference on NOAA-16

No interference effects were seen for the STX-1 or STX-3 high-gain antennae, or the STX-2 or STX-4 omni-directional antennae. Small biases were seen for the STX-2 high-gain antenna in channel 17: 1.2 K for the space view and 0.4 K for the internal target view. Earth-view biases are difficult to quantify for this window channel, but it was estimated that overall brightness temperature errors are within approximately ±0.5 K when the transmitter is active (Atkinson, 2000). As the error due to RFI for AMSU-B on NOAA-16 is within the instrument noise level, no correction was applied, unlike for all other AMSU-B instruments. It is important to limit the use of N16 data, and in particular the harmonization, to the periods identified by in Figure 9 of Hans et al, 2017.

4.6.3 RF Interference on NOAA-17

Channel 19 is affected by both STX-2 and STX-3. STX-2 mainly affects the space view (~90 counts, or 5 K). STX-3 affects both space view (1 K) and Earth view (3.5K in center of scan). Correction tables have been provided for removal of the resulting biases. This is much less than the interference experienced with NOAA-15, so the uncertainty of the correction should be smaller and on the other hand the reason for the large bias for

channel 19 in the center of scan is not clear, and the bias does not increase linearly with transmitter power. These are results from ground tests. The maximum Earth view bias is 2K for Channel 19 and 1K for Channel 18 in flight according to the KLM User Guide.

It is very difficult to estimate the uncertainty introduced by RF Interference for N16 and N17, we estimate, very approximately, 0.5 K. (Ricketts and Atkinson 1998)

4.7 Model assumptions

The +0 term in the main equation, Eq 3-1, considers the following effects:

- Non-quadratic nonlinearity
- Variable nonlinearity coefficients

Burgdorf et al. (2018) describe how the Moon can be used for investigations of the performance of microwave sounders in flight.

5 Harmonisation

Harmonisation is described separately, so only a brief overview is considered here. The harmonisation coefficients are listed in Section 3.1.5. The harmonisation process will determine these parameters, and a covariance matrix for the parameters. To propagate these uncertainties through to the uncertainty associated with the Earth radiance we need the sensitivity coefficients:

$$\frac{\partial L_E}{\partial q_{nl}} = \frac{1}{g_E}\frac{(C_E - \bar{C}_S)(C_E - \bar{C}_{IWCT})(L_{IWCT} - L_S)^2}{(\bar{C}_{IWCT} - \bar{C}_S)^2}$$

$$\frac{\partial L_E}{\partial \alpha} = \frac{(L_{MIWCT} - \hat{L}_{E,i})(\cos(2\vartheta_{E,i}) - \cos(2\vartheta_S))}{2g_E} \quad \textit{Eq 5-1}$$

$$\frac{\partial L_E}{\partial \Delta T_C} = \frac{\bar{C}_{IWCT} - C_{E,i}}{g_{E,i}(\bar{C}_{IWCT} - \bar{C}_S)}\left(1 + \frac{2q_{nl}(C_{E,i} - \bar{C}_S)(L_{IWCT} - L_S)}{(\bar{C}_{IWCT} - \bar{C}_S)}\right) \quad \textit{Eq 5-2}$$
$$(1 - \frac{\alpha}{2g_{E,i}}(\cos(2\vartheta_{E,i}) - \cos(2\vartheta_S)))$$

Eq 5-3

$$\frac{\partial L_E}{\partial g_S} = -\frac{1}{(1 - g_S - g_{Pl})^2}[L_{ME} - g_{Pl}L_{Pl} + L_{CMB}(g_{Pl} - 1)] \quad \textit{Eq 5-4}$$

$$\frac{\partial L_E}{\partial g_{Pl}} = -\frac{1}{(1 - g_S - g_{Pl})^2}[L_{ME} - g_S L_{CMB} + L_{Pl}(g_S - 1)] \quad \textit{Eq 5-5}$$

$$\frac{\partial L_E}{\partial L_{CMB}} = -\frac{g_S}{1 - g_S - g_{Pl}}$$

$$\frac{\partial L_E}{\partial L_{Pl}} = -\frac{g_{Pl}}{1 - g_S - g_{Pl}}$$

Note that the harmonisation coefficients will be correlated with each other and the result of the harmonisation process will include a covariance matrix for these. In order to propagate uncertainties, the

full law of propagation of uncertainties, including the correlation term, is required. Note that the harmonisation coefficients will be the same for all time with one sensor.

A Appendix on detailed information about uncertainty components

A.1 Noise

The noise in the measurement of Earth views, DSV and IWCT views is accounted for by looking into the variations of the recorded counts. As noise estimate, we use the Allan Deviation, calculated for each of the four DSV and IWCT views separately from scan line to scan line. Taking the average over the K=4 views and over N=300 scan lines, we obtain about eight estimates per orbit of the count noise in DSV and IWCT view for each channel. This calculation has been done for the overall noise analysis described in Hans et al. (2017) for all instruments and periods to get an overview of the evolution of the noise. For the production of the FCDRs, the calculation is carried out on the fly, after filtering out single scan lines of bad data. Also, for the calibration of the instrument, the IWCT and DSV counts used for one scan line are a rolling weighted average over seven scan lines. Taking into account this rolling average procedure further reduces the noise in counts according to the law of uncertainty propagation. The noise in Earth counts is calculated by rescaling the raw (i.e. no weighted average considered) count noise in DSV and IWCT according to the temperatures of cosmic microwave background and internal calibration target, as well as the earth counts recorded for each pixel. Some exemplary values of the count noise from MHS on Metop-B are:

DSV: u_$\bar{C}$_S for ch1-5: 12, 24, 22, 18, 14 Counts

IWCT: , u_$\bar{C}$_IWCT for ch1-5: 16, 27, 29, 22, 17 Counts

Earth : u_C_E for ch1-5: 34, 63, 65, 49, 37 Counts

The spectrum of the noise has been investigated for some instruments and periods. It varies among the instruments, channels and years, but it is mostly a dominant white noise component or a mixture of pink and white noise. This result supports our use of the Allan Deviation between scan lines instead of between adjacent views, because variations in the noise on scan line to scan line time scales, relevant for the calibration cycle of the MW instruments, are captured by the scan line to scan line Allan Deviation. In contrast, using the Allan Deviation between adjacent views produced smaller count noise values in cases of strong pink noise component and will therefore underestimate the uncertainty of the radiance due to count noise for these cases.

The analysis of the noise performance over the life time of all considered instruments has revealed that the noise on counts may vary strongly on monthly scales, but it is rather stable when considering the whole life time of the instrument and it does not cause steady degradation of the instrument

A full analysis and discussion of the noise is presented in (Hans et al., 2017).

As example we show the result of propagating the uncertainty due to noise in the Earth counts through to the final measurand, the brightness temperature (for MHS channels 1 and 3).

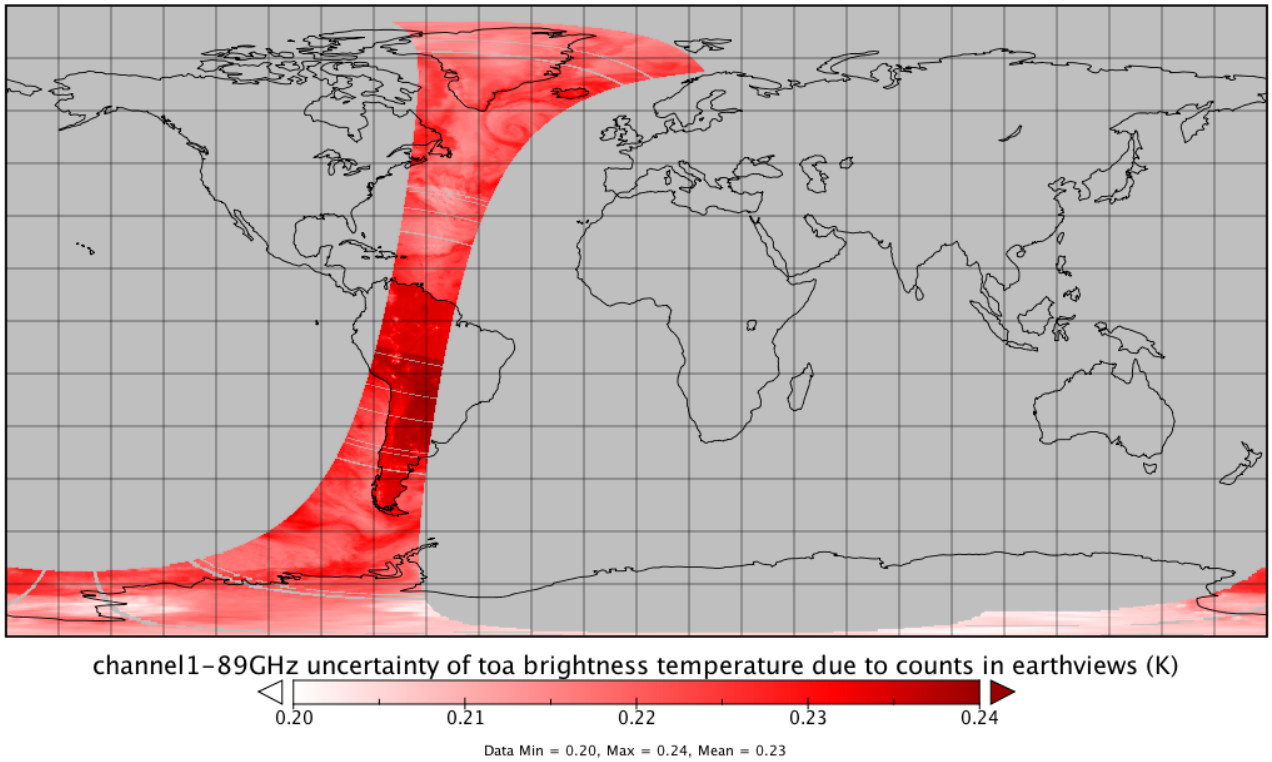

Figure 2 Half an orbit of MHS on Metop-B on 04-04-2014: The uncertainty in the brightness temperature in channel 1 due to the uncertainty in earth view counts is shown.

For every 300 scan lines we have an estimate for the count noise on DSV and IWCT view. The count noise for the earth views per pixel and scan line is obtained by rescaling the DSV and IWCT count noise of the corresponding scan line, according to the recorded scene brightness temperature of each pixel. This earth view count noise (the typical range for MHS on Metop-B is given above) is multiplied by the sensitivity coefficient to obtain the resulting uncertainty in radiance. The uncertainty in brightness temperature is then obtained by multiplying by the partial derivative of brightness temperature with respect to radiance.

The 300-scan line windows for which the DSV and IWCT count noise has been estimated shine through in the uncertainty of the brightness temperature in Figure 2 with discrete steps from one window to the next: e.g. over South America, there is a small step in the noise of 0.004 K from 0.238 K to 0.242 K. The scene dependence (channel 1 is a surface channel) of the earth count noise is captured well: For warmer regions (e.g. South America) the noise is higher than for colder regions (Antarctica). In Figure 3, the same uncertainty is shown for channel 3 (water vapour channel): the uncertainty due to count noise in earth views is almost twice as large as for channel 1.

Grey stripes in the swath indicate missing uncertainty information due to bad data that is not suited for uncertainty estimation.

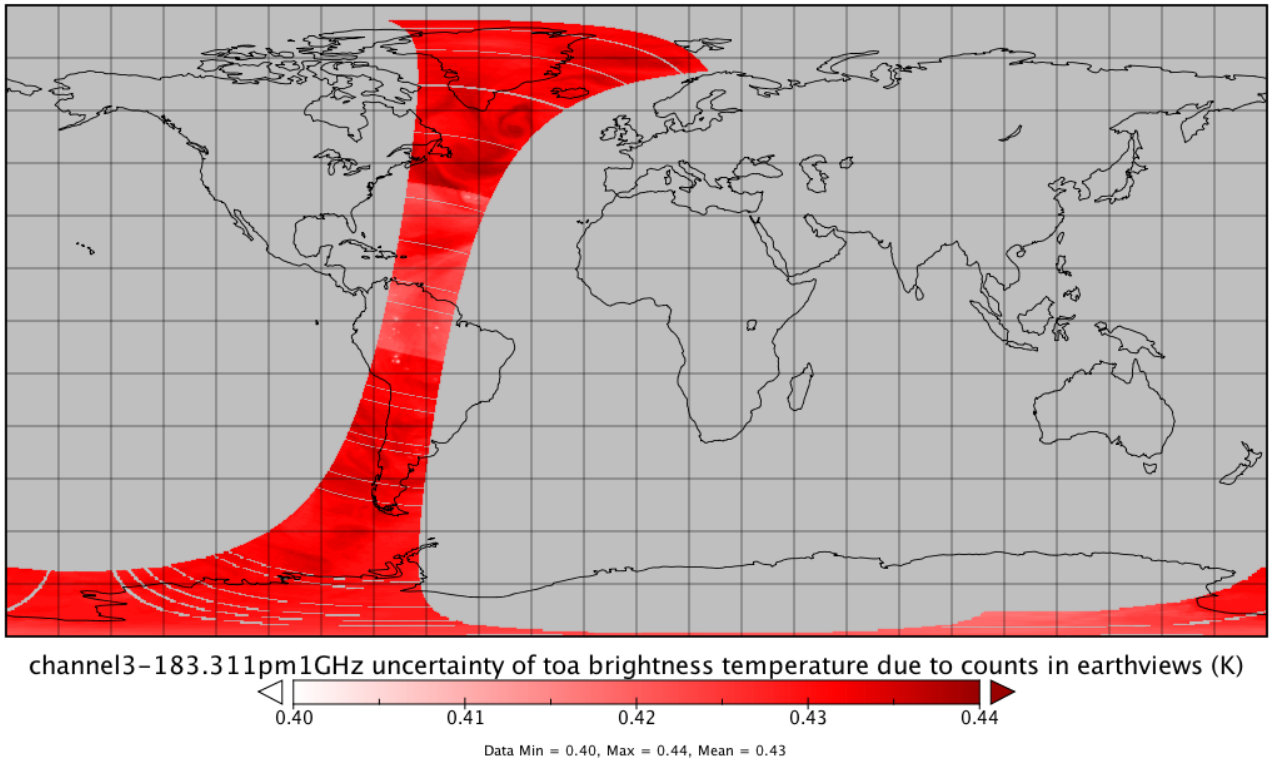

Figure 3 Half an orbit of MHS on Metop-B on 04-04-2014: The uncertainty in the brightness temperature in channel 3 due to the uncertainty in earth view counts is shown.

A.2 Internal warm calibration target radiance effects

A.2.1 Internal warm calibration target temperature measurement

The temperature of the internal warm calibration target is calculated as the weighted mean of temperatures $T_{\mathrm{PRT},i}$ measured by the m PRTs (two for SSM/T-2, seven for AMSU-B and five for MHS), the values of which are available from the Level-1-b file.

$$T_{\mathrm{IWCT}} = \frac{\sum_{k=1}^{m} w_k T_{\mathrm{PRT},k}}{\sum_{k=1}^{m} w_k} + 0 \qquad \text{Eq 5-6}$$

The weights are chosen based on confidence in the different PRTs. The +0 here represents the assumption that the mean PRT signal is equal to the temperature of the IWCT averaged over the field of view of the radiometer.

The PRTs are arranged as shown in Figure 4. Normally, the weights are 2 for the sensor in the centre and 1 for the others. Depending on the result of quality checks on the PRT sensors, the weights of bad sensors are set to zero. As long as there are more than two usable PRT sensors, the PRT measurement for this scan line is accepted. If there are only two or fewer useable PRT measurements for this scan line, the closest good scan line for PRT measurements is taken. This procedure defines the initial temperature of the IWCT for the current scan line. The final temperature that is assigned to the current scan line is obtained by a weighted,

rolling average over seven adjacent scan lines (three before, three after the current one). This final temperature enters the measurement equation as the IWCT temperature.

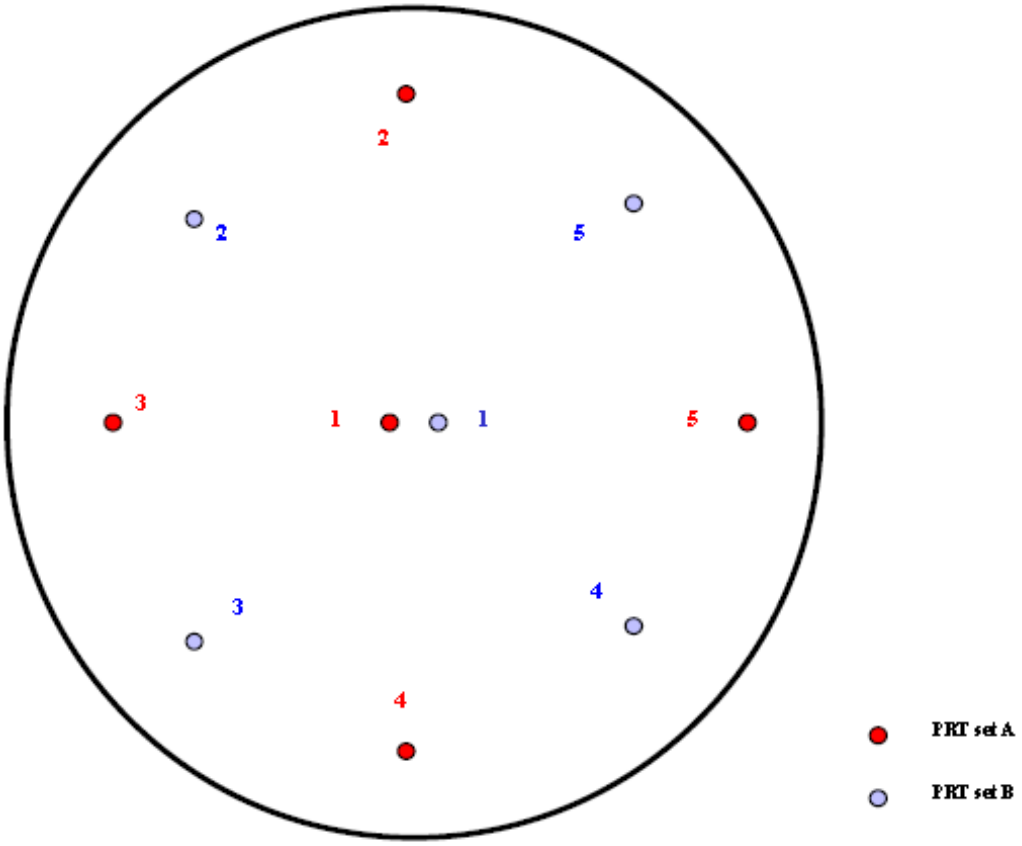

Figure 4 Primary (set A, red) and secondary (set B, blue) set of PRT in the IWCT of MHS, as seen from the bottom of the instrument. AMSU-B has got two PRTs more in a similar alignment (a regular hexagon with one PRT in the center).

A.2.2 IWCT emissivity

The IWCT was designed to approximate a blackbody as closely as possible using a pyramidal structure. The emissivity of the target is at least 0.9999 and is likely to be higher than this. Gencorp, Aerojet (1990) quote an emissivity of 0.9999992 and 0.9999979 at 89 GHz and 150 GHz respectively for the IWCT of AMSU-B.

An emissivity this high is achieved predominantly through the pyramidal structure and only to a smaller extent due to the coating. This means that the coating must degrade significantly before any emissivity change is apparent and therefore the error in emissivity due to target degradation can be considered negligible.

Furthermore, with an emissivity this high, there is no significant reflection from the target and therefore we do not need to worry about radiation from the local oscillator or other sources reflecting from the target.

A.2.3 Absolute calibration accuracy and equivalence for a single PRT

The uncertainty associated with the PRT measurement is related to the quality of the pre-flight calibration. There will have been an initial calibration uncertainty for these parameters and these effects could drift over time – the PRT response changes as the PRT ages. This drift is discussed with thermal gradients, below.

The long-term accuracy of a PRT is estimated to be 0.1 K, based on conversations with NPL's thermometry experts. It is possible that one or more PRTs undergoes some fundamental change that creates a step change in its reading that is greater than this. Ground tests, on the other hand, suggest a better accuracy than 0.1 K (Atkinson & Ricketts, 1994). This is discussed along with thermal gradients in the following section.

Any contact thermometer will measure its own temperature. It is the job of the engineer to ensure that its temperature is the same as the temperature that should be measured. For the PRTs on the IWCT this was done by embedding the thermometers within the IWCT (to provide good thermal contact). It is unlikely that there is a significant uncertainty associated with the positioning of an individual PRT.

A.2.4 IWCT thermal gradients and PRT drifts

The temperature measured by the Microwave sensor is an average temperature over the IWCT. The use of multiple PRTs is to account for any thermal gradients across the IWCT; the average temperature is expected to be close to the temperature measured by the Microwave Sensor (Figure 4). Note however that there are times when this may not be the case, for example when weight zero is assigned to a PRT, or a PRT did not pass the median test. If in the latter case the large deviation of one PRT from median is due to an actual thermal gradient, then the brightness temperature of the blackbody would be off by about 30mK (threshold of median test - 0.2K - divided by the number of PRTs, i. e. seven in case of AMSU-B).

MHS is equipped with three precision resistors, which are used to eliminate the effect of slow variations in the voltage of the power supply. These variations cause systematic errors, because the resistance of the PRT is determined as the ratio of the assumed voltage and the measured current. The precision resistors are used to verify the value of the assumed voltage. Their values are included in the data packets (in counts).

As the targets are insulated from external thermal swings and the entire instrument is thermally insulated from the platform, the temperature variations across the targets are usually small (less than ±0.05 K). Spatial trends larger than 0.2K, however, can be identified from comparing the values of certain PRTs to the average values of the others (see Figure 5, Figure 6) and can be present for years with certain satellites. Secondly, there could be a vertical temperature gradient in the pyramid structure, which cannot be measured. A thermal model has been developed in order to estimate the size of the vertical temperature gradient (Hewison, 1991). He concludes that the worst errors are less than 30mK and recommends that no correction for thermal gradients through the absorber is made.

When these differences are observed over time it is clear that the differences between PRTs increases, an upper limit of the lifetime drift of the temperature sensors can be estimated from the scatter among the temperatures measured on the blackbody at different times (see

Figure 7 and 8). Given the fact, however, that there are estimates of the stability of the temperature sensors based on measurements on ground, we consider these numbers more realistic (see section A2.3).

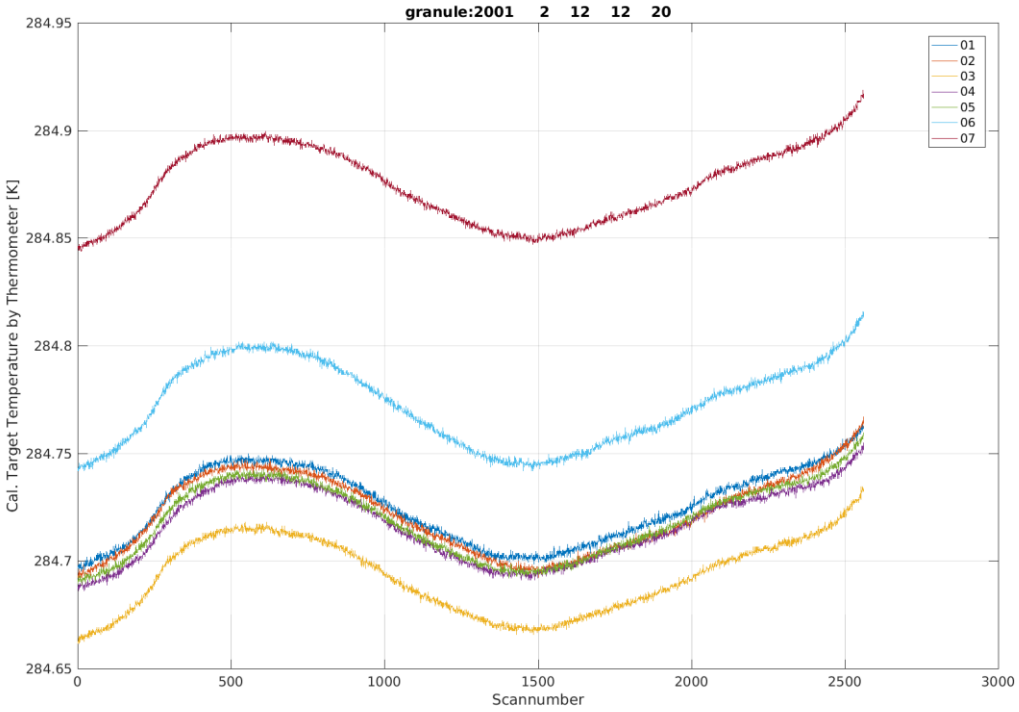

Figure 5 The temperatures measured with the PRTs during one orbit of AMSU-B on NOAA-16 on 2/12, 2006. The PRTs are arranged in the shape of a hexagon with PRT1 in its centre (analogous to Figure 4, where the PRTs of MHS are shown as arranged in a square). The side with PRT6 and PRT7 seems to have the highest temperature.

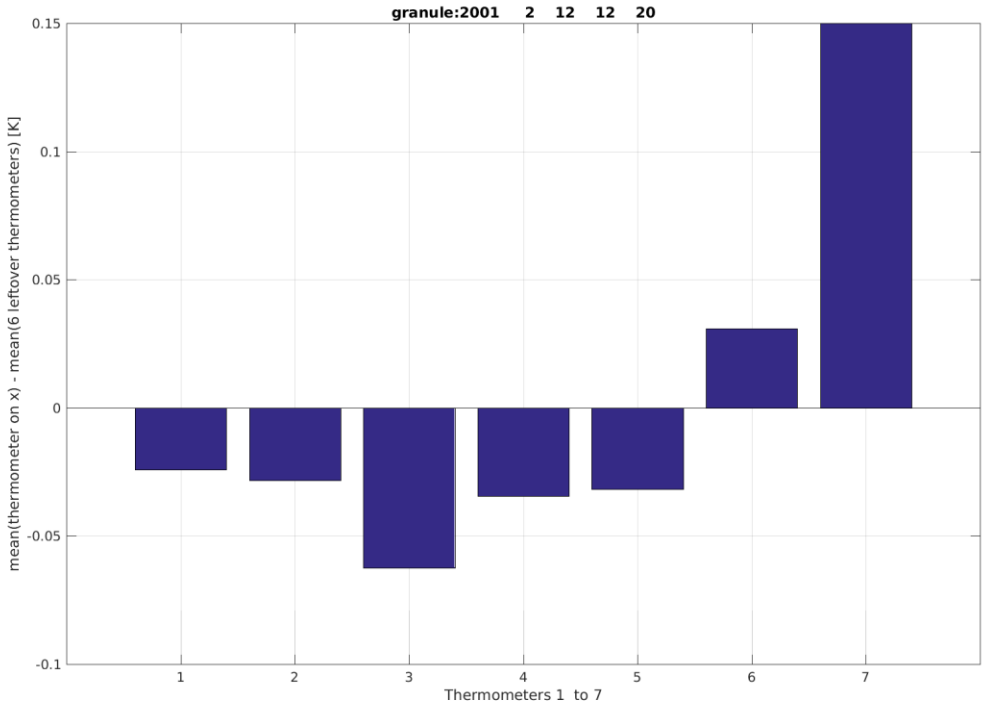

Figure 6 The temperature differences from the mean measured with the PRTs during one orbit of AMSU-B on NOAA-16 on 2/12, 2006. This plot is an alternative representation of Fig. 5, which illustrates the fact that the side with PRT6 and PRT7 seems to have a temperature above average.

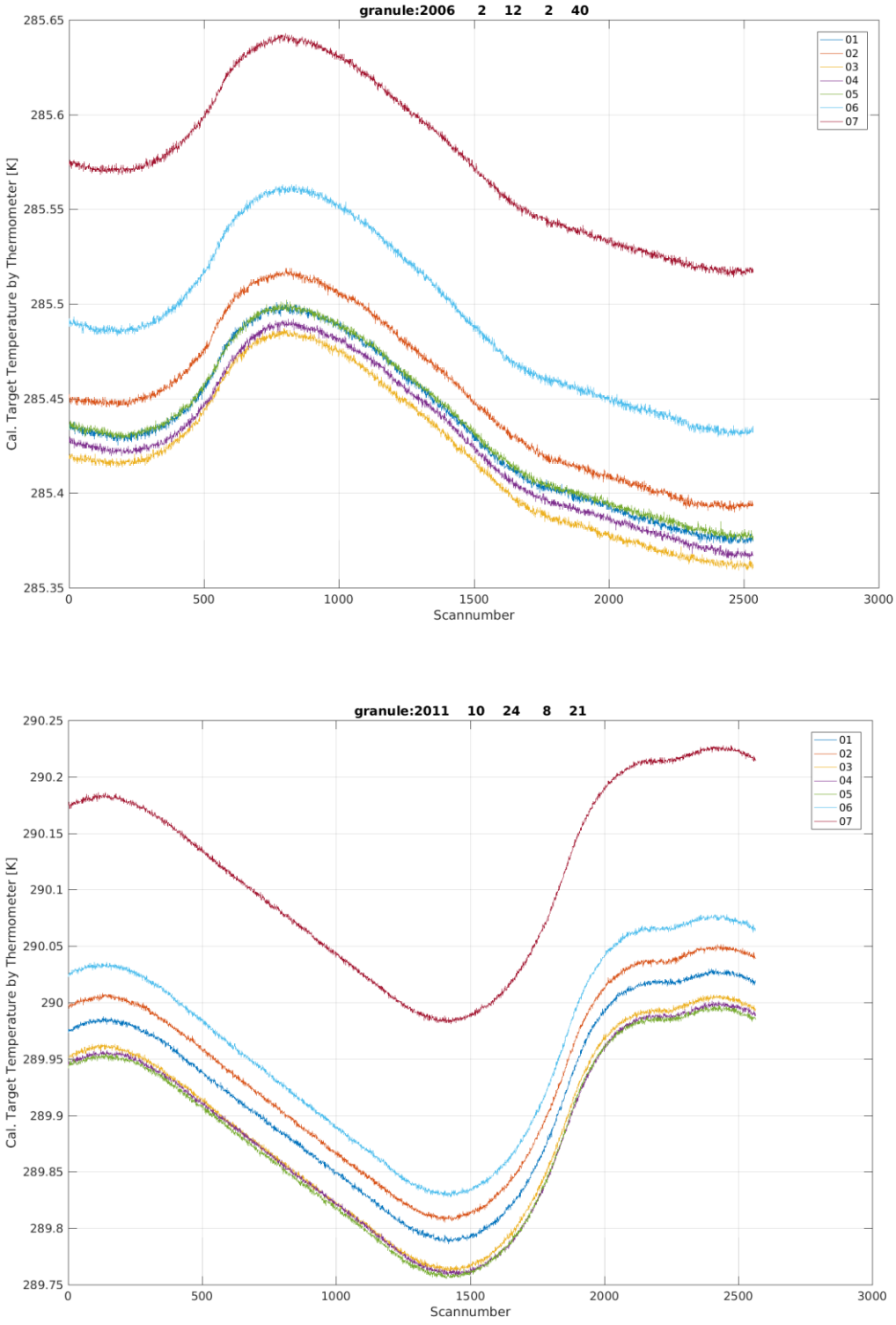

Figure 7 The temperatures measured with the PRTs during orbits of AMSU-B on NOAA-16 on 2/12, 2006 (top) and 10/24, 2011 (bottom). PRT 1, in the central position, gave within 0.01 K the same temperature reading as 3, 4, and 5, in the year 2006, whereas five years later the difference to the other PRTs has doubled. Compare also to Fig. 6 for the changes happening before 2006.

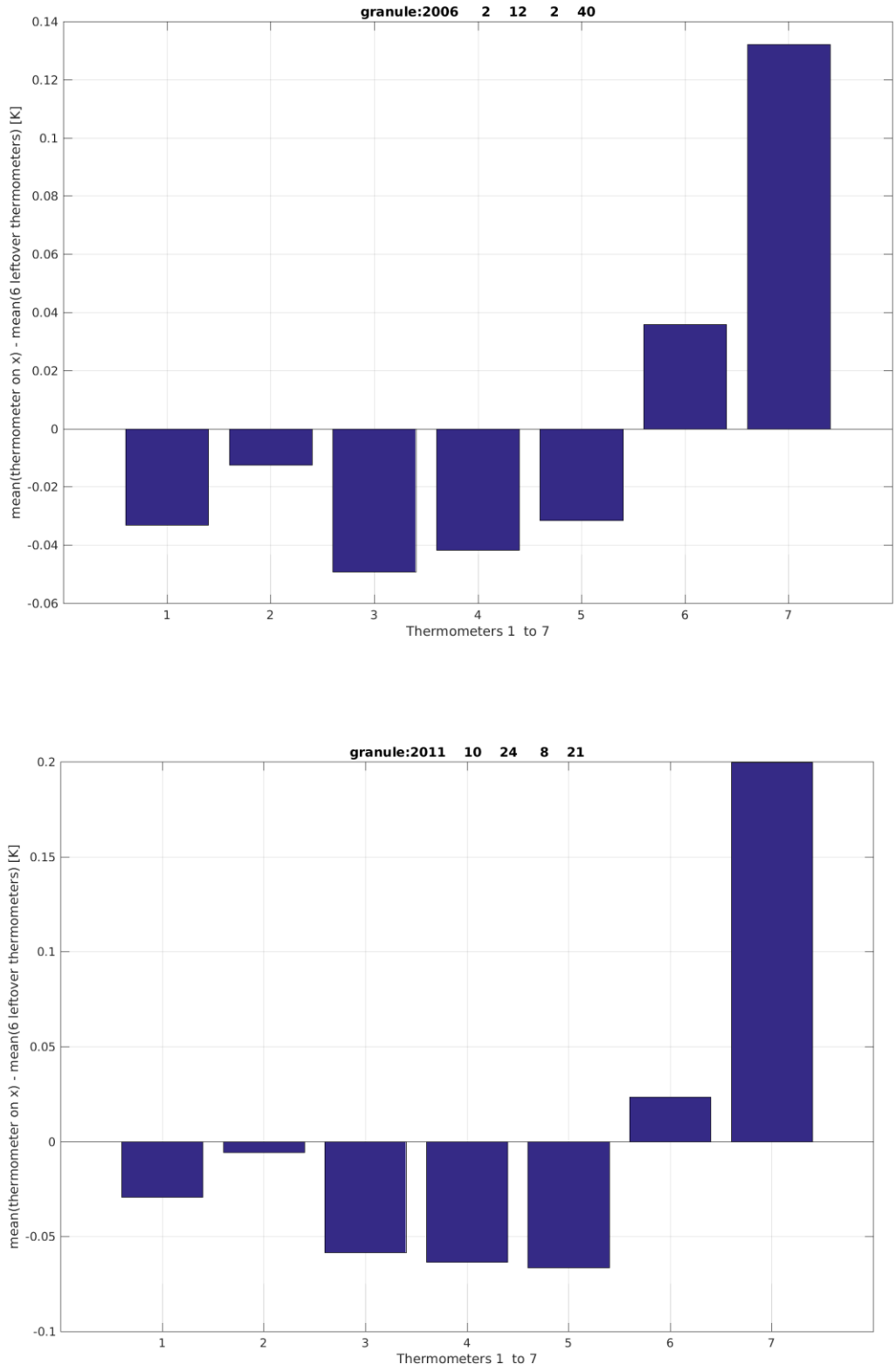

Figure 8 The temperature differences from the mean measured with the PRTs during orbits of AMSU-B on NOAA-16 on 2/12, 2006 (top) and 10/24, 2011 (bottom). PRT 1, in the central position, stayed at some 0.03 K below the mean of all other PRTs. PRT 7, however, which had been constant at about 0.14 K above the mean between 2001 and 2006, was 0.2 K above the mean of all others in 2011 and 0.23 K above the median, which is represented by PRT 1.

A 2.5 PRT noise

There will also be simple noise in the PRT temperature measurements – variations in the measured signal due to random fluctuations. These were determined from the measurements themselves, taking the systematic temperature variations over an orbit into account.

The noise in the PRT measurements is estimated with the Allan Deviation. As for the IWCT and DSV views, we calculate separately for the five PRTs the Allan Deviation for 300 scan lines. Afterwards the average over the five PRTs is taken (it is in the range of 0.084 K for MHS on Metop-B for a single PRT and a single measurement). Taking into account the rolling average further reduces the noise to about 0.04 K in this example. The noise is smaller for AMSU-B, typically 2.4 mK (single PRT, single measurement).

A.3 Error of Viewing Angles for polarisation

The pointing requirement for Nadir, Earth pixel 1, Earth pixel 90, and Space view is 0.12° with MHS, but the ground tests of the PFM revealed non-compliances in the V axis (out of scan plane, i. e. not relevant for the polarisation correction). In most cases, however, the success criteria of 0.09° were fulfilled. Assuming that the pointing error is the same in A and V axis, we obtain a systematic error of $0.09°/\sqrt{2}=0.06°$ for the scan direction.

The specification for co-registration performance is 0.07° and was met in the ground tests for the PFM. There were no non-compliances with FM2.

In-orbit verification of MHS spectral channels co-registration with FM5 gave deviations of up to 0.06° in the along-track (cross-scan) direction (Bonsignori, 2017).

The beam pointing requirement for AMSU-B is ±0.1° for all channels according to the KLM User's Guide. Checking this value in flight with AMSU-B on NOAA-16 gave an average difference of 0.11° between the measured pointing and the one calculated with AAPP in the scan direction (Burgdorf et al., 2018).

The OV tests of AMSU-B Proto-Flight Model (NOAA-15) showed that the scan mechanism was operating with SD figures being less than 0.01°. A random uncertainty of 0.04° for Earth view and 0.02° for space view was calculated from data obtained in the operational situation of MHS on MetOp-B.

A.4 Harmonisation coefficient: Cold space bias correction

The temperature of the cosmic microwave background (CMB) gives the signal in the DSV. However, there is radiation from earth or the platform that enters the sidelobes. Therefore, as for the correction of the earth views for contamination by deep space and platform, we also need a correction of the DSV (see Eq. 3-7). This correction is given as temperature in Kelvin for every channel and every space view configuration (one configuration is chosen at the beginning of the mission) in the clparams.dat file of the AAPP and in the header of the Level-1b files. This cold space bias correction temperature is added to the temperature of the CMB. The values of this cold space bias correction vary significantly among the different space view configurations, channels and instruments. We do not know the reason for the choice and changes of values: e.g. for MHS on NOAA-18, all channels and space view configurations have the same correction, whereas for Metop-B, only channel 3 and 4 have the same values, the others differ. Also, the space view configurations 1 and 3 are equal whereas configurations 0 and 2 differ for Metop-B.

In our processing we use the values assigned to the corresponding instrument and configuration (the information on which configuration is chosen is available in the header). Here, we show an example of MHS-

Metop-B data: Comparing our results in brightness temperature to the brightness temperature obtained from the AAPP-7-13 processing, we see systematic deviations (see Figure 9). For colder scenes the deviation is large, for warmer scenes (close to the temperature of the blackbody), the deviation is small. This hints at a problem with the signal of the DSV and therefore possibly with the cold space bias correction. This is also hinted at by the fact that channel 1 is quite different from the others, channel 3 and 4 have the same correction values and similar trend in deviation and channel 2 and 5 are rather similar in both deviation from AAPP and correction values.

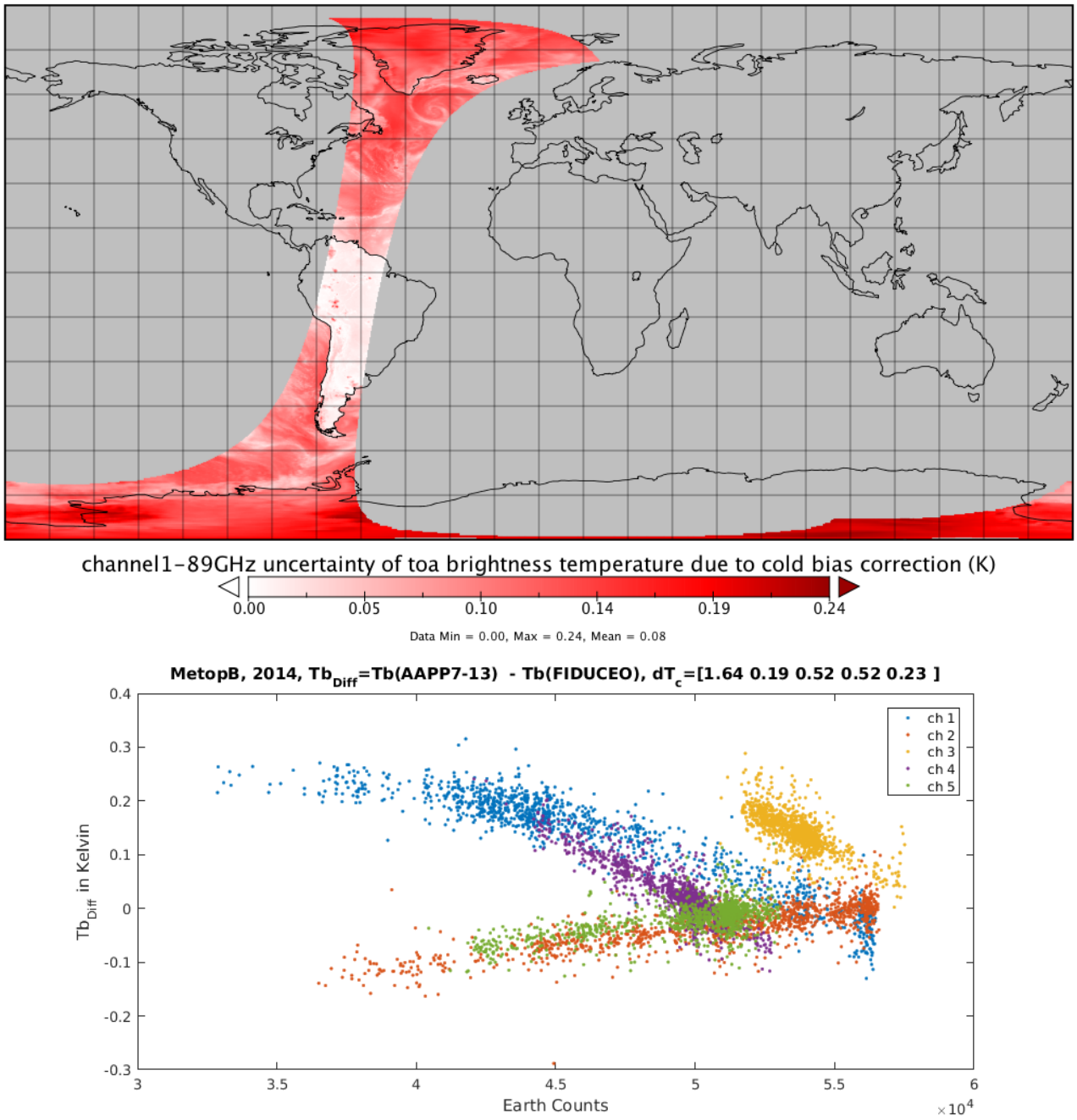

Figure 9 Difference in brightness temperature of AAPP 7-13 and current FIDUCEO processing plotted against the earth counts (only nadir pixel). For colder scenes (smaller number counts) the deviation gets larger.

Since the origin of the cold space correction values listed in the clparams.dat file and the header of the Level1-b file is unclear, and we now see a difference between our processing and AAPP7-13, we think it is

possible that this AAPP7-13 processing uses another set of correction values. Optimizing this correction as harmonisation parameter might shed light onto this issue. To evade interaction with the optimisation of the other harmonisation coefficient for the antenna pattern correction of earth views, it might be useful to first restrict the optimisation of the cold space bias correction to the nadir pixels where the antenna pattern correction of earth views is zero anyway.

The propagation of the uncertainty of this cold space bias correction is considered in our processing as follows: The spread of the given values (in clparams.dat file and L1b-header) for the correction serves as first guess of possible uncertainty on the correction. Therefore, taking the standard deviation over all channels and configurations for one instrument (here: MHS on Metop-B) we obtain 0.6 K. Multiplying this input uncertainty with the sensitivity coefficient of the radiance to the cold space bias correction, and further transforming to sensitivity of the brightness temperature, yields the final uncertainty in brightness temperature due to uncertain cold space bias correction. It is shown in Figure 10 for channel 3. For channel 3, the uncertainty range does not fully cover the range of deviation. The trend is captured however. Hence, the assumed uncertainty of 0.6 K of the correction is too small to explain the deviations in brightness temperature.

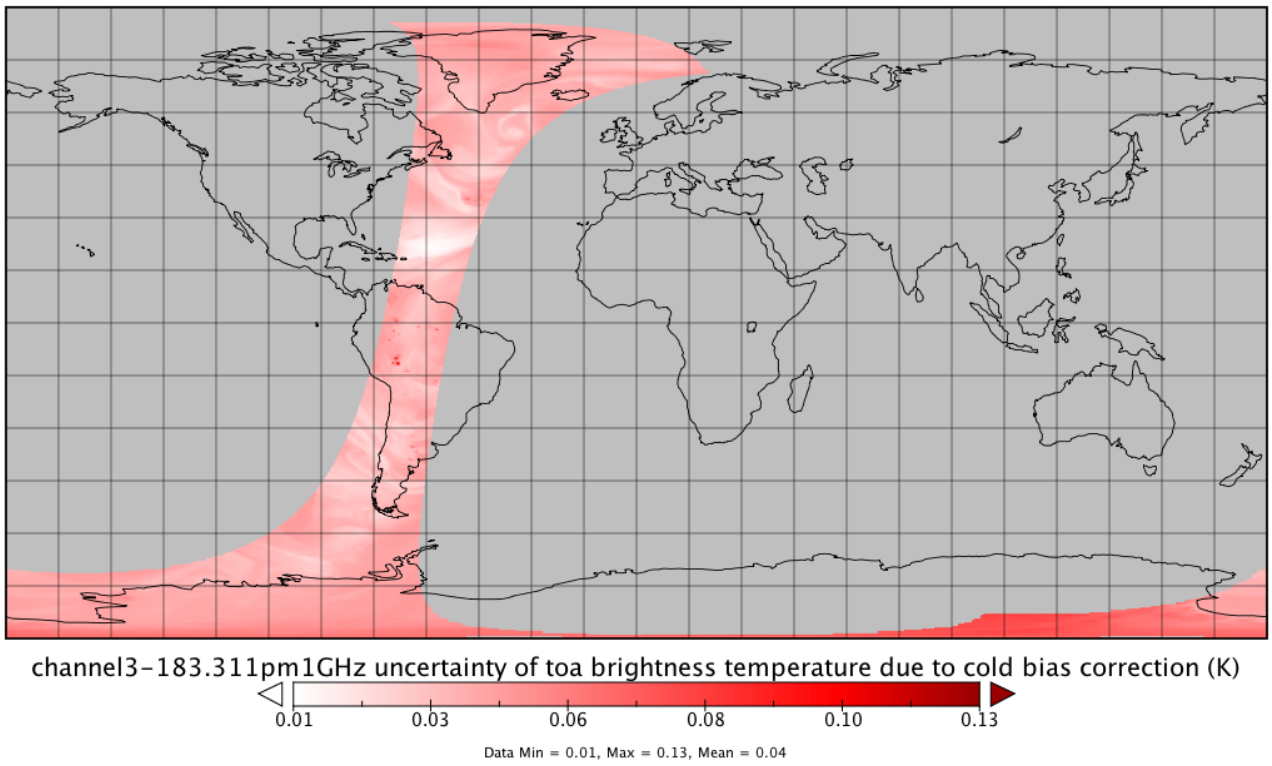

Figure 10 Uncertainty of the brightness temperature in channel 3 due to uncertainty in cold space bias correction. In warmer regions, where the influence of the DSV measurement is small, the uncertainty generated in the brightness temperature due to uncertain cold space bias correction is small. In these warm regions, the AAPP and FIDUCEO processing do not differ either.

A.5 Radiance of platform

The radiance of the platform, adding up with the radiation of cold space and of earth to the complete measured radiance in the fundamental measurement equation (Eq. 3-1) is unknown. It is not known what the "platform" is either: It could be parts of the MHS/AMSU-B instrument itself or some part of the satellite.

It is not trivial to give a temperature and corresponding radiance for this term L_{Pl}. One would need the complete knowledge of the geometry of the instrument on board the satellite in order to know what "the platform" should be. Further, one would need information on temperature of the platform, i.e. these parts seen by the side lobes. These parts of the satellite and/or instrument do not necessarily have the same temperature as one of the various housekeeping sensors of the instrument itself. Also, the temperature of the platform's components may have large orbital variations.

AAPP assumes that the "platform" simply reflects the radiance of the Earth pixel that is currently observed. This is a strong assumption: Even if the platform has a reflectivity of one, it is not clear what part of the Earth (or which Earth pixels' radiance) should actually be reflected into the side lobes of the antenna.

The opposite extreme would be to assume that the platform fully reflects the cold space radiance. Investigating this issue with our FCDR processing, we obtain a maximum change of 0.22K for channel 1, when using the cold space radiance for the platform compared to using the earth radiance of the current pixel. Channel 1 has the largest antenna correction factors according to the fdf.dat file for MHS on Metop-B. Channel 3 has a much smaller correction. Any change in the assumed radiance of the platform has therefore only little impact: We obtain 0.03K as maximum change compared to the AAPP assumption of using Earth radiance for the contribution of the platform. The two figures below show the difference in the final brightness temperature obtained for the earth pixels for the two assumptions: Brightness temperature for "radiance of platform = radiance of earth" minus brightness temperature for "radiance of platform = radiance of cold space".

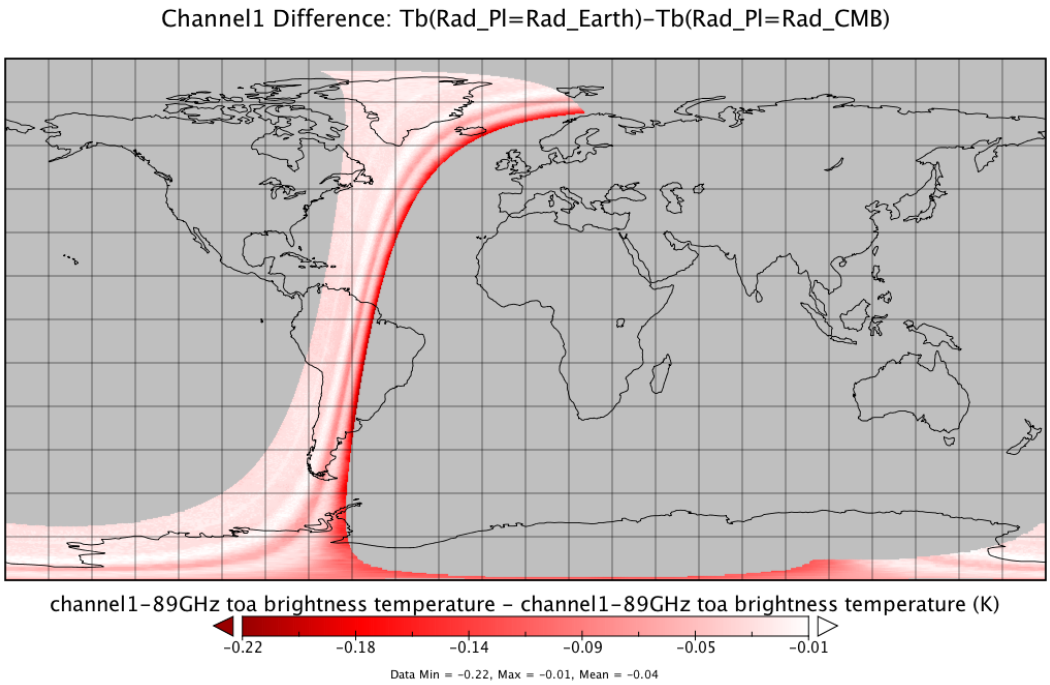

Figure 11 Difference of Earth pixel brightness temperatures from two evaluations of the measurement equation: 1. Evaluation follows the assumption made in AAPP, i.e. radiance of Platform = Radiance of Earth", 2. Evaluation assumes "radiance of Platform =Radiance of Cold Space". This figure shows the result for Channel1 1. Maximum difference of the evaluations is -0.22 K at the edge of the swath.

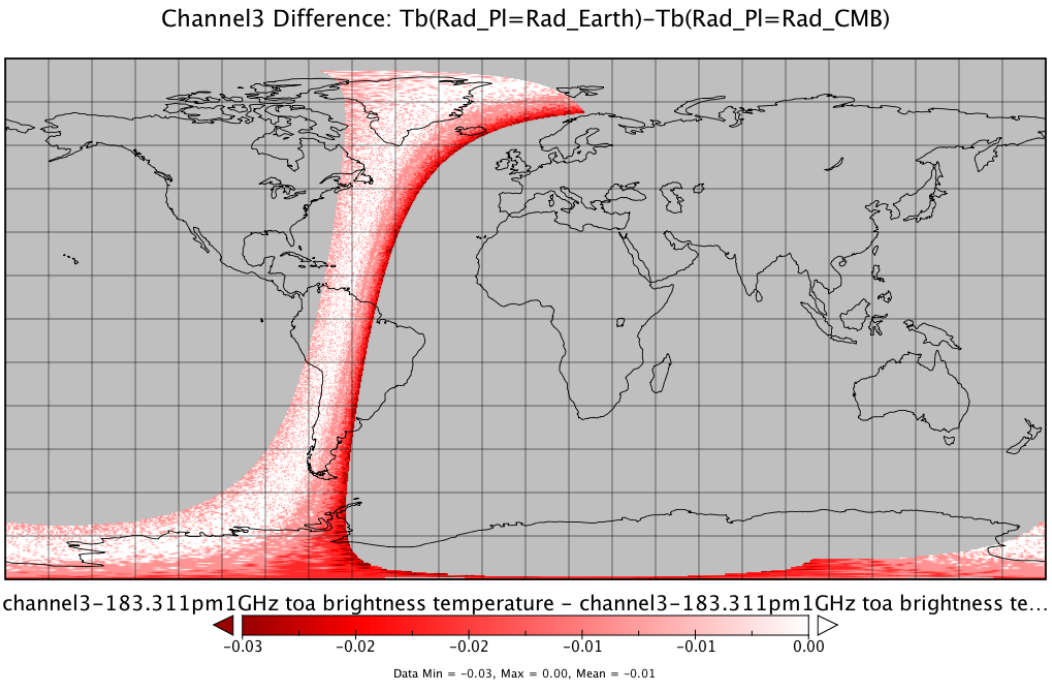

Figure 12 Same as for Figure ; showing channel 3 here. Maximum difference is -0.03K at the edge of the swath.